City, University of London Institutional Repository

This is the accepted version of the paper.

This version of the publication may differ from the final published version.

Learning to Detect 3D Rectal Tubes in CT Colonography using a Global Shape Model

Xiaoyun Yang, Gareth Beddoe, and Greg Slabaugh

Medicsight PLC, Kensington Centre, 66 Hammersmith Road, London, UK
`{xiaoyun.yang}@medicsight.com`

Abstract. The rectal tube (RT) is a common source of false positives (FPs) in computer-aided detection (CAD) systems for CT colonography. In this paper, we present a novel and robust bottom-up approach to detect the RT. Generative models, trained using kernel density estimation (KDE) on simple low-level features, are employed to rank and select the most likely RT tube candidate on each axial slice. Then, a shape model, robustly estimated using RANSAC, infers the global RT path from the selected local detections. Our method is validated using a diverse database, including data from five hospitals. The experiments demonstrate a high detection rate of the RT path, and when tested in a CAD system, reduce 20.3% of the FPs with no loss of CAD sensitivity.

Keywords: Rectal Tube, RANSAC, CAD, CT colonography

1 Introduction

The RT has a (potentially bent) cylindrical shape and includes a bulbous tip that often has a polyp-mimicking appearance. As such, the rectal tube is a common source of false positives generated by the CAD for CT Colonography (CTC) [1–4]. To improve the overall CAD performance, it is therefore desirable to have a robust and efficient way to identify the RT and remove its resulting FPs from the CAD marks presented to the reader. Some research has been proposed [2–4] to address this problem. Iordanescu *et al.* [2] developed an image segmentation based method that detects, via template matching, the air inside the RT in the first nine CT slices, tracks the tube, and performs segmentation using morphological operations. Suzuki *et al.* [3] employed a Massive Training Artificial Neural Network (MTANN) to distinguish between polyps and FPs due to the RT. Barbu *et al.* [4] detected part of the RT using Probabilistic Boosting Tree (PBT) and then applied dynamic programming to find the best RT segmentation from the detected parts. Both MTANN and PBT are supervised training discriminative techniques, however, their training heavily relies on the features of individual samples at each slice. None of the previous methods make use of a global shape model of the RT.

In this paper, we propose a novel and robust approach for the detection of the RT. We have two major contributions: (i) a generative model trained on simple low-level features to detect 2D potential locations of the RT; (ii) a global

Fig. 1. Rectal Tube Detection Scheme.

3D shape model estimated using RANSAC [5] that robustly infers the path of RT from local (and potentially outlier) detections. To our best knowledge, this is the first approach to combine simple low level detections with a global shape model for the robust detection of the RT. The method is computationally inexpensive and reliable. The results demonstrate a high detection rate using a diverse dataset, and in a CAD system, achieve a 20.3% reduction of false positives without any loss of sensitivity.

2   Method

2.1   Overview

We present a learning framework to combine generative models for low level detection of air in the rectal tube with a global shape model of the RT path. The overview of the system is presented in Figure 1. We start with simple image processing, applied to each 2D axial slice, to detect air regions (RT candidates) within the body in the most caudad slices, starting at the anal verge and moving up the abdomen towards the lungs. For each RT candidate, three simple low level features are computed: the normalized spatial position x and y of the centroid and the size h of the region. A generative model using kernel density estimation is trained for prone and supine data respectively and then used to rank the RT candidates. In each slice, the most probable tube candidate is selected and the others are discarded. From these 2D detections, RANSAC fits a global 3D global shape model representing the RT path. RANSAC is a robust statistical technique that can infer the real RT path even in the presence of strong outliers resulting from incorrect KDE predictions. The following subsections describe each of these steps in detail.

2.2   Generative models for 2D candidate detection of RT regions

In this section we demonstrate how we generate local 2D RT candidates, and train a generative model from simple low-level features. The generated model is then employed for selection of the most probable candidate on a given slice.

The air region in the RT can be identified on an axial image slice using standard image processing techniques. First, we apply simple thresholding using a threshold value of -750 HU. All the air pixels then belong to the background

and all the remaining pixels are assigned to the foreground pixels; the largest foreground region will be the body. The air regions within the body region are then extracted using morphological operations. Furthermore, a 3D bounding box around the body is determined.

Each candidate is represented by its centroid (C_x^i, C_y^i, C_z^i). Three low level features, (V_x^i, V_y^i, V_s^i), for each candidate are computed: the normalized spatial position (V_x^i) and (V_y^i) in the x and y direction, and the region size (V_s^i). The normalized spatial positions are determined as $V_x^i = (C_x^i - rect_{left})/rect_{width}, V_y^i = (C_y^i - rect_{bottom})/rect_{height}$, where $rect_{width}$ and $rect_{height}$ define the width and height of the bounding box, $rect_{left}$ and $rect_{bottom}$ represent the minimum bounding box coordinate in x and y, respectively.

In the training stage, each candidate is sorted by the distance from its centroid (C_x^i, C_y^i, C_z^i) to the annotated RT center point in the same slice. The candidate with the smallest distance is selected as training data to build a generative model if the distance value is less than $6mm$ and the size is between 0.5 and 130mm^2. If the size is too large, the candidate may correspond to or be combined with non-tube air regions. The selected feature data (V_x^i, V_y^i, V_s^i) is then used to build a generative model with KDE. From the constructed KDE, the probability of a given feature vector can be estimated as

$$P(T|(V_x, V_y, V_s)) = \begin{cases} \frac{1}{C} \sum_{i=1}^{n} e^{-\frac{(V_x - V_x^i)^2}{2h_x^2}} \sum_{i=1}^{n} e^{-\frac{(V_y - V_y^i)^2}{2h_y^2}} & \text{if } V_s \in [0.5, 130]\text{mm}^2 \\ 0 & \text{otherwise} \end{cases}$$

(1)

where (V_x, V_y, V_s) is a given feature vector, (V_x^i, V_y^i, V_s^i) $(i = 1, .., N)$ is the ith example used for training. If V_s is too big or too small, a penalty is given and the probability is zero. C is a normalization factor that can be set to 1 as we are only interested in a ranking of the candidates' probability values. The KDE model is generated from prone and supine data separately using Gaussian kernels with bandwidth 0.25 both in x and y direction.

In the testing stage, we apply the appropriate (prone or supine) generative model to the candidate's feature vector. A probability can then be estimated for each RT candidate. The candidates are ranked by the estimated probability and only the one with the maximum value in each slice will be selected. Figure 2 (a) shows an example CT image, (b) the candidate regions and (c) most likely candidate selected by the KDE model.

The length of the RT within the body may vary depending upon how deeply the RT is inserted. We use the most $120mm$ caudad of CT slices as our processing range which are enough to cover the RT in our experiment data. The majority of RT is located in the most $90mm$ caudad of CT slices. Examples of RT detections are shown for two CT scans in Figure 3 for 120 consecutive slices in which the depth resolution is $1mm$. In the figure, the red circles (inliers, usually corresponding to the RT) and blue dots (outliers, typically not corresponding to the RT) illustrate the selected candidate centroids, plotted separately, i.e., in the xz and yz planes. The tube is present in the patient for the most caudad
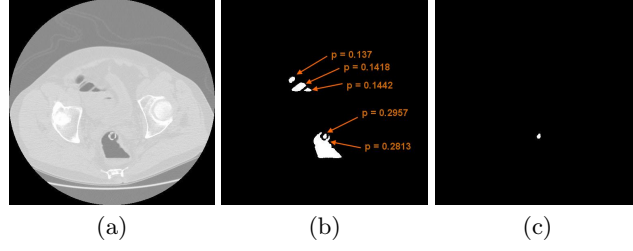
Fig. 2. Examples of the candidate selected by KDE. (a) the CT image, (b) the candidate regions, and (c) the region selected by KDE. This region corresponds to the air in the RT.
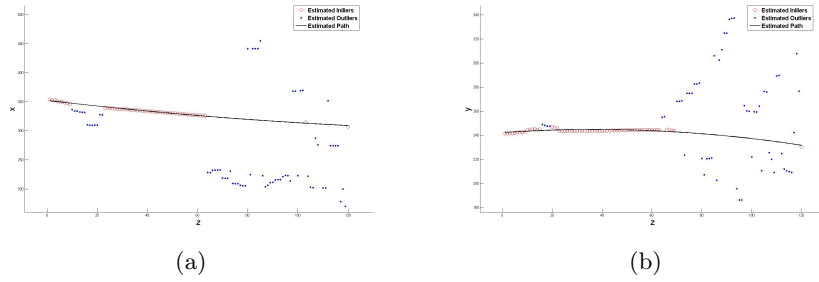

Fig. 3. Examples of RANSAC fitting of two scans in the xz and yz planes.

slices with lower z value. Ideally, the KDE would predict all the air regions of the RT; however, KDE can wrongly pick up the candidates from other structures. Numerous outliers are shown in the figure, particularly near or past the end of the tube (approximately on slice $z = 60$ for the examples in the figure). In other cases the RT air regions may connect with colon air and the centroid can deviate away from true locations.

2.3   RT path estimation using a global shape model

In this section we describe how the underlying RT path is inferred from the RT candidate centroids selected in the previous step.

The RT is a cylindrical tube placed in the patient's colon, and once the colon is insufflated with room air and there is no force to twist the RT. The path of the RT can be approximated as a quadratic curve (which includes a straight line as a special case). While there may occasionally be some other air-filled structure or noise giving a quadratic path, the RT is easily identified as the longest path along a smooth and continuous quadratic curve starting at the bottom of the patient. To estimate the correct RT path, one must differentiate the outliers from the inliers that represent the true locations of the RT. From the inliers, we

can infer the other 2D RT locations missed by KDE. With the prior model of the global shape information that the RT path is a quadratic curve and continuously appears in the most caudad slices, we use that as a criteria to seek a maximum set of inlier points that can fit the quadratic curve which can be resolved by RANSAC [5], as show in Equation 2:

$$\hat{\theta} = \arg\max_{\theta} \sum_{i=1}^{N} f(e_i^2|\theta) \tag{2}$$

where

$$f(e_i^2|\theta) = \begin{cases} 1 & e_i^2 < \delta^2 \\ 0 & \text{otherwise} \end{cases} \tag{3}$$

where θ is the quadratic model to be estimated. e_i is the error or the distance between the data V_i and the estimated curve. δ is a threshold under the hypothesis that the error is generated by a true inlier contaminated with a Gaussian noise $P[e_i \leq \delta]$, where we expect the value of P is 0.95. A 3D space curve quadratic in z models the path as $[C_x(z), C_y(z), z]^T = [\theta_{0x} + \theta_{1x}z + \theta_{2x}z^2, \theta_{0y} + \theta_{1y}z + \theta_{2y}z^2, z]^T$, where the estimation of $[\theta_{0x}, \theta_{1x}, \theta_{2x}]$ and $[\theta_{0y}, \theta_{1y}, \theta_{2y}]$ is performed separately in the xz and yz planes respectively using RANSAC. In Figure 3, the blue dots represent the candidate locations classified as outliers (non-RT locations) and red circles represent the candidate locations classified as inliers (RT locations). The black line illustrates the inferred RT path from the inliers. Even in the presence of large outliers (non-RT locations) generated by KDE, the estimated RT path is quite reliable. After RANSAC fitting, given a slice number, we can predict the RT path location. RANSAC can be viewed as a method to achieve a robust regression to fit the global shape model to data containing significant outliers.

3   Results

Our experiment evaluates the RT tube detection for suppression of FPs in CAD. In this experiment, the CT colonography data consisted of 199 patients of prone and supine series (398 CT scans) collected from 5 institutions. CT images were generated using scanners from all the major manufacturers, including Siemens, GE, Philips, and Toshiba, with 4, 8, 16, 32, and 64 multi-slice configurations, KVp ranged from $120-140$, and exposure ranged from 29 - 500 mAs. All subjects were scanned within the last 10 years (1999 - 2008) and roughly 80% were administered fluid and fecal tagging. Any detection by CAD is removed as a FP if the in-plane distance between the center of the detected region and the center of the detected RT is less than $6mm$. The CAD produced 2186 false positive detections, of which 444 were removed by RT detection, from 5.49 to 4.37 per scan. Overall, this improved the CAD with a 20.3% FP reduction. None of the true positives detected by the CAD were missed due to RT detection, therefore CAD sensitivity was unaffected.
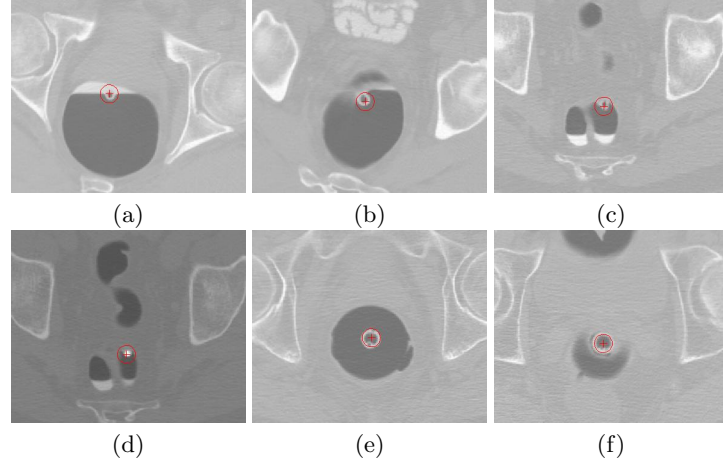
Fig. 4. Examples of detected RTs scanned from different hospitals.

4   Discussion and Conclusion

In this paper, we presented a novel and robust learning approach for RT detection and removal of its resulting FPs in CAD. The approach starts from simple image processing operations and simple low-level 2D feature extraction for locally detected objects, which are then probabilistically ranked using KDE. Then, RANSAC robustly estimates the RT path from the most likely 2D candidates by fitting a 3D global shape model. Our RT detection method has shown a high performance for detecting the RT path and removing FPs in CAD. In future work, we plan to investigate robust approach to detect the RT tip along the estimated path and its radius which can help remove FPs more reliably.

References

1. Slabaugh, G., Yang, X., Ye, X., Boyes, R., Beddoe, G.: A Robust and Fast System for CTC Computer-Aided Detection of Colorectal Lesions. Algorithms **3**(1) (2010) 21–43
2. Iordanescu, G., Summers, R.M.: Reduction of false positives on the rectal tube in computer-aided detection for ct colonography. Medical Physics **31**(10) (2004) 2855–2862
3. Suzuki, K., Yoshida, H., Nppi, J., Dachman, A.: Massive-training artificial neural network (MTANN) for reduction of false positives in computer-aided detection of polyps: Suppression of rectal tubes. Medical Physics **33**(10) (October 2006) 3821–24
4. Barbu, A., Bogoni, L., Comaniciu, D.: Hierarchical part-based detection of 3D flexible tubes: Application to CT Colonoscopy. In: MICCAI (2). (2006) 462–470
5. Fischler, M.A., Bolles, R.C.: Random sample consensus: a paradigm for model fitting with applications to image analysis and automated cartography. Commun. ACM **24**(6) (1981) 381–395